Development of Sensory-motor Fusion based Manipulation and Grasping Control for a Robotic Hand-Eye System

Yingbai Hu, Zhijun Li, *Senior Member, IEEE*, Guanglin Li, *Senior Member, IEEE*, Peijiang Yuan, Chenguang Yang, *Member, IEEE*, and Rong Song

***Abstract*—In the paper, sensory-motor fusion based manipulation and grasping control has been developed for a robotic hand-eye system. The proposed hierarchical control architecture has three modules: vision servoing, surface electromyography (sEMG) based movement recognition, and hybrid force and motion optimization for manipulation and grasping. A stereo camera is used to obtain the 3D point cloud of a target object and provides the desired operational position. The AdaBoost-based motion recognition is employed to discriminate different movements based on sEMG of human upper limbs. The operational space motion planning for bionic arm and force planning for multi-fingered robotic hand can be both transformed as a convex optimization problem with various constraints. A neural dynamics optimization solution is proposed and implemented online. The proposed formulation can achieve a substantial reduction of computational load. The actual implementation includes a bionic arm with dextrous hand, high-speed active vision, and a EMG sensors. A series of manipulation tasks consisting of tracking/recogniting/grasping/ of an object are implemented and tested, and experiment results exhibit the responsiveness and flexibility of the proposed sensory motion fusion approach.**

Keywords: bionic arm, multi-fingers hand, sEMG, quadratic programming, vision servoing

I. Introduction

Robotic bionic arms and prosthesis hands become very useful in helping people with severe physical disabilities, which could enable disable people to achieve greater independence and consequently increase quality of life [1], [2], [3]. In generally, bionic arms and prosthesis hands can be controlled by a joystick, which enables an operator to perform manipulation, open/close of fingers, and thus offers an intuitive interface. However, the bionic arm control loop short of biological signals feedback makes it very tedious to perform simple manipulation, e.g., safely picking up, holding, or releasing an object. Therefore, it is necessary to investigate the replacement of the natural hand with a bionic arm and prosthesis hand using a close-to-natural human-machine interface. Humans are extremely adept at controlling the high degree of freedom hand-wrist-arm musculo-skeletal system and are able to grasp and manipulate objects according to task requirements with a minimum of effort. It is of great interest to study human manipulation and grasping behaviour in order to extract underlying principles which may be transferred to robotic or prosthetic devices.

Myoelectric control allows a convenient human-machine interface by transforming electromyography (EMG) signals into control outputs. Two control approaches are currently employed in conventional myoelectric control: direct control and pattern recognition (PR). Direct control links antagonistic muscles or muscle groups directly to a single degree-of-freedom (DoF) [4], and [20]. Various switching methods have been presented for sequentially transition between different DoFs or functions in finite state machines [5]. These simplistic controllers provide reliable performance, but lack the functionality to smoothly operate multiple DoFs [6].

PR methods utilize machine learning techniques, including both classification [7] and regression [8], to decode a mapping between myoelectric inputs and desired outputs [21], which enhances functionality compared to direct controls by enabling multiple DoFs without explicit switching methods. However, increased functionality requires an updated training set which is highly dependent on the users motion repeatability [7] and may be influenced by many external factors [9], [10], [11]. Thus, the decoding often overfits to a small set of the full input space, and performance tends to degrade over time [12].

An improvement method to the PR is combining concepts of visual servoing (VS). These visual servoing-based methods extend pattern recognition principles to multiple DoFs through linear transformations between sensor inputs and control outputs, naturally providing both simultaneous and proportional control. The mapping creates a redundancy in the control scheme which reduces the precision needed in muscle activations to control the entire task-space.

Visual servoing is defined as the use of visual feedback mechanisms for the kinematic control of a robot. Based on the positioning of the camera on the link and control techniques,

This work is supported in part by National Natural Science Foundation of China grants Nos. 61573147, 91520201, and Guangzhou Research Collaborative Innovation Projects (No. 2014Y2-00507), Guangdong Science and Technology Research Collaborative Innovation Projects under Grant 2014B090901056, Guangdong Science and Technology Plan Project (Application Technology Research Foundation) No. 2015B020233006, and National High-Tech Research and Development Program of China (863 Program) (Grant No. 2015AA042303). Corresponding author: Zhijun Li.

Y. Hu and Z. Li are currently with College of Automation Science and Engineering, South China University of Technology, Guangzhou, China. Email: zjli@ieee.org.

G. Li is with Shenzhen Institutes of Advanced Technology Chinese Academy of Sciences Shenzhen, Guangdong, China. Email: gl.li@siat.ac.cn.

P. Yuan is with Robotics Institute, Beihang University, Beijing, China, Email: itr@buaa.edu.cn.

C. Yang is with Zienkiewicz Centre for Computational Engineering, Swansea University, SA1 8EN, UK. Email: cyang@theiet.org.

R. Song is with Department of Medical Engineering, Sun Yat-Sen University, Guangzhou, China. Email: songrong@mail.sysu.edu.cn.

VS ramifies into several types. Eye-in-hand and eye-to-hand VS are represented by the position of the camera on the robotic manipulator. Being attached on the robot arm, eye-in-hand VS provides a narrower field of view as compared to eye-to-hand servoing. Many control schemes use either a direct visual servoing or a dual loop system [19], [31]. A visual processing method for human tracking using intelligent wheelchair was developed in [19], and a visual servoing for stabilization of an nonholonomic mobile robot was proposed by incorporating a model predictive control [31].

An important issue in controlling a bionic arm combining a multi-fingered robotic hand for object manipulation and grasping is the synthesis of the optimal motion planning and contact force such that the planning trajectory and contact forces are guaranteed under the stability of the manipulation and grasping and its feasibility. This problem, known as motion-force optimization (MFO) can be formulated as a constrained optimization problem. Due to computational time of finding the solution, the MFO is usually performed off-line. However, during the execution of a manipulation task, the planning trajectory of the arm and the position of the contact points on the object, or the wrench (force and moment) to be balanced by the contact forces, may change with time and cannot be planned in advance. The planning trajectory and contact forces must be compatible with the various constraints depending on the joint velocity, the type of contact, as well as on the joint torque limits of every joints. In these cases, suitable algorithms for online computation of the solution of the constrained MFO problem must be devised. The utilization of recurrent neural networks is investigated in [22], [23], where the friction constraints and the joint torque limits were considered. In [34], an approach was proposed for computing optimal grasping and manipulation forces, which utilizes neural network to learn the nonlinear inverse kinematics functional relating the hand joints positions and displacements to object displacement.

In this paper, sensory-motor fusion based manipulation and grasping control for a robotic hand-eye system are developed. The proposed hierarchical control architecture has three modules: vision servoing, sEMG-based movement recognition, and hybrid force and motion optimization for manipulation and grasping. The contributions can be summarized as follows:

(i) The AdaBoost-based motion recognition is proposed to discriminate different movements based on sEMG of the multi-fingers;
(ii) The operational motion planning for bionic arm and force planning for multi-fingered robotic hand is both transformed as a convex optimization problem with various constraints. A neural dynamics optimization solution is proposed and suitable to be implemented online.

The actual implementation utilizes a bionic arm with dextrous hand, high-speed active vision, and a EMG sensors. A series of manipulation tasks consisting of tracking/recogniting/grasping/ of an object are implemented and tested, and experiment results demonstrate the responsiveness and flexibility of the proposed sensory motion fusion approach.

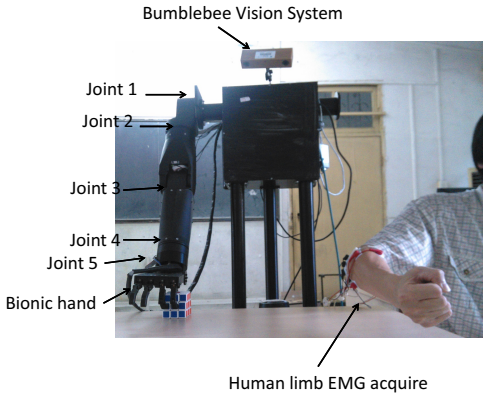

Fig. 1. The mechanical design of the bionic arm and hand.

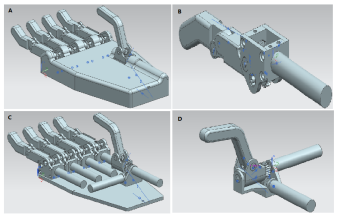

Fig. 2. Design of dexterous hand: A. The whole view of the hand; B. One finger; C. The inside view of hand chamber; D. Thumb with 2 DOFs

II. Bionic Arm System

The developed bionic arm is shown in Fig. 1, which consists of five revolute joints: one for each shoulder abduction-adduction, shoulder flexion-extension (flx-ext), elbow flx-ext, and wrist flexion-extension (flx-ext), wrist pronation-supination (pron-sup). The DC motor selected to activate robotic articulations was a Maxon dc flat brushless motor EC90 for the joint 1 and EC45f for other joints, respectively, and harmonic transmission drives are used ((model SHD-17-100-2SH for joints 1 and 3, model SHD-14-100-2SH for joints 2, 4, 5)). The physical parameters are listed in Table 1. In the robotic device, high-resolution encoders (1024 pulse/cycle) and Hall effect sensor are used to measure the displacement angles between the joints.

In Fig. 2, the hand is approximately the same as human-hand in size and shape. It comprises of five fingers (including one thumb) and a DOF in the thumb in the roll axis, which is suitable for stably grasping an object of arbitrary shape. Each finger except the thumb consists of two joints, the lower one is an active joint, the upper one is an passive joint. The active joint is driven by an DC motor through worm gear through Maxon controller to control its motion (see Fig. 3). The passive joint is driven by a linkage, its joint rotation range is limited by the active joint. The motion of the passive joint derives from the natural motion of human hand. The palm is constructed with five aluminum plates connected with screws. The finger can be mounted on the palm directly. Through the four holes located at the rear plate in the palm, the hand can

TABLE 1
THE PARAMETERS OF BIONIC ARM AND DEXTEROUS HAND

Joints	Torques (Nm)	Range(degree)
Shoulder (flx-ext)	44.4	-90 –90
Shoulder (abd-add)	2.46	-150–150
Elbow (flx-ext)	8.27	-90 –90
Wrist (pron-sup)	2.46	-150–150
Wrist	2.46	-120–120
Thumb	0.13	0–56
Index & Middle finger (Ring and Litter Finger)	0.13	0-66

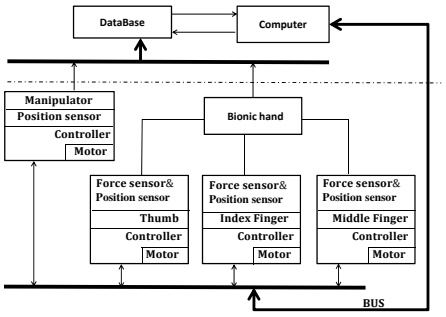

Fig. 3. The control architecture of the hand.

be attached to the bionic arm.

III. VISION FEEDBACK CONTROL SYSTEM

A. Visual Sensor Preprocessing and its projection model

The machine vision processing adopt a Point Grey Bumblebee2 stereo camera with IEEE-1394 Firewire connection. The Point Grey Bumblebee2 stereo camera is a 2 sensor progressive scan CCD camera with fixed alignment between the sensors. Video is captured at a rate of 20 fps with a resolution of 640×480 to produce dense colored depth maps to assist in tracking and a viable pose estimation of the object. The resolution-speed trade-off has to be managed concisely as an increased frame speed gives a smooth robot trajectory whereas enhances the processing time. And an increased resolution provides a denser, more accurate point cloud for feature extraction but with increased latency. In this paper, the adopted projection model is shown in Fig. 5.

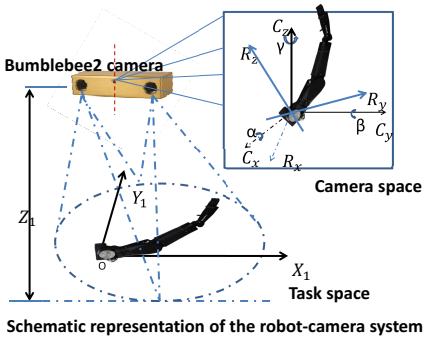

Fig. 4. The structure of the vision sensor.

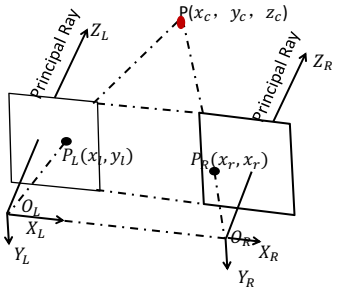

Fig. 5. The front view of vision localization.

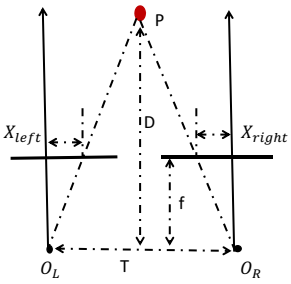

Fig. 6. The vertical view of vision localization.

Camera calibration is necessary as the use of lenses introduces nonlinearities and deviates from the simple pin-hole model such as lens distortion, namely radial and tangential distortion. The camera parameters, namely, the intrinsic, extrinsic and distortion are evaluated by using a 2D checkerboard pattern. 3D reference models were avoided due to computational complexity and high cost of precise calibration objects. In this paper, 20 checkerboard images were fed to the calibrator algorithm encompassing differential angles in the projection space. This provides enough values to estimate the camera geometry parameters [18].

B. 3D Reconstruction

The images captured by the Bumblebee2 stereo camera in active ambient lighting are shown in Fig. 7. Both the images are calibrated using the camera intrinsics and are corrected for distortion. Subsequently, the undistorted images are stereo rectified in order to align the epipolar lines of both the projection planes and ensure the presence of similar pixels in a specified row of the image. The images obtained are then frontal parallel and are ready for correspondence estimate. The essential and the fundamental matrix are calculated by using Epipolar geometry. The essential matrix is a 3×3 matrix with 5 parameters; two for translation and three for the rotation values between the camera projection planes. On the other hand, the fundamental matrix represents the pixel relations between the two images and has seven parameters, two for each epipole

and three for homography that relates the two image planes. Bouguets algorithm is then implemented to align the epipolar lines and shift the epipoles to infinity.

Stereo correspondence is a method of matching pixels with similar texture across two co-planar image planes. The distance between the columns of these perfectly matched pixels is defined as $d = x_l - x_r$, where x_l is the column value of left image pixel, and x_r is the column value of right image pixel. The vertical view is shown in Fig. 6.

Block matching is implemented to evaluate the correspondence between the images. Block sizes of 15 pixel window are used to find the matches by the use of SAD (sum of absolute differences). Semi-global method is used to force the disparity values to the neighboring pixels for a more comprehensive result. Disparity is inversely proportional to the depth of the pixel and is related by the Triangulation equation

$$D = T\frac{f}{d} \tag{1}$$

where f is the focal length, d is the disparity, and T is the baseline.

Triangulation refers to the estimation of depth of an object by visualizing its location from two different known points. The reconstruction of the image in the Cartesian co-ordinates is obtained by the use of projection matrix evaluated using Bouguets algorithm. The 3D reconstruction of the robots workspace:

$$Q\begin{bmatrix} x, & y, & d, & 1 \end{bmatrix}^T = \begin{bmatrix} X, & Y, & Z, & W \end{bmatrix}^T \tag{2}$$

where D is the depth, Q is the projection matrix, X, Y, Z, and W is the coordinates.

C. Object Detection

In the paper, color based segmentation is used in order to separate a single color object from the background, we choose the red color as a sign of object. The image is converted into $L \times a \times b$ color space and the Euclidean distance between red-green and yellow-blue opponent components of the object and a and b matrices calculated, [27], [28]. Here, represents the L^* luminance component, while a^* and b^* represent color components. The formulae for converting an RGB image into the coordinates can be found in previous works (e.g. and). The minimum value gives the most accurate estimate of the object. In the color space, the Euclidean distance between $(L_1{}^*, a_1{}^*, b_1{}^*)$ and $(L_2{}^*, a_2{}^*, b_2{}^*)$ can be defined as

$$\Delta E_{ab} = \sqrt{(L_2{}^* - L_1{}^*)^2 + (a_2{}^* - a_1{}^*)^2 + (b_2{}^* - b_1{}^*)^2} \tag{3}$$

which is approximately equivalent to the perceptual difference between these two colors. Furthermore, the corners of the red-object are calculated by Harris corner detector and the centroid calculated by intersection of the diagonals. The depth value of the centroid is then extracted from reconstructed point cloud of the task space.

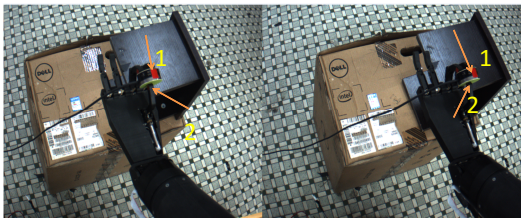

Fig. 7. The object landmark.

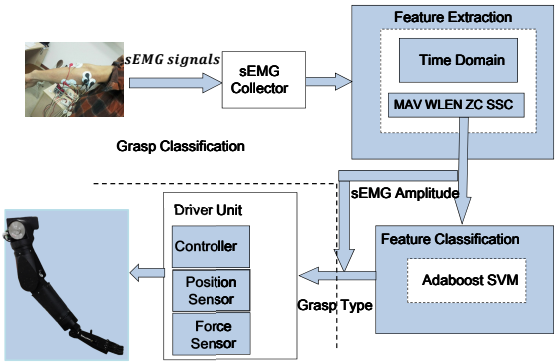

Fig. 8. Schematic diagram of the bionic hand grasping based on sEMG.

IV. EMG BIO-FEEDBACK SERVO STRUCTURE

In this section, in order to perform the grasping of dexterous hand, we employ EMG signal as control feedback and the real-time EMG motion recognition can be implemented for controlling the dexterous hand, [20], [26]. Fig. 8 shows the schematic diagram of grasping manipulation using EMG signals. The fundamental components are the EMG acquisition, feature extraction unit, and the classifier unit. The adopted classification is AdaBoostSVM.

A. Data Acquisition

There are many types hand/wrist motions when studying the dextrous hand. In daily life, all the hand motion can be simplified as three types: hand closing (HC), hand opening (HO) and finger pinching (FP), shown in Fig. 9. Four surface electrodes were used to acquire the sEMG signals from the extensor digitorum, flexor digitorum superficialus, extensor carpiradialis, and flexor carpiulnaris, respectively, which are related with the three motions. In order to collected high quality sEMG signals, the skin was scrubbed with alcohol and shaved if necessary, and then the electrodes with conductive gel were attached to the corresponding positions.

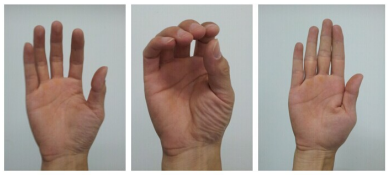

Fig. 9. Three postures of the grasping hand.

In this paper, four groups of sEMG signals were collected from one intact-limb subjects forearm. The four groups were used for the training section. We collected sEMG signals of each hand and each posture constitutes a subset. The subject is asked to perform the three gestures. The subject hold his posture 7 seconds and repeat 7 times.

B. Feature Extraction

In order to control a robotic hand in real time without perceiving a time delay, the processing time of sEMG pattern recognition should be less than 300 msec. Thus, the scheme of a sliding window with an incremental window is adopted for the steady-state motion recognition. For the real-time myoelectric hand control, all the processes including transmitting control commands should be completed within an incremental window. In this study, a 64-msec (64 samples) sliding window with a 16-msec (16 samples) incremental window is selected. After data segmentation, fourteen features would be extracted in a sliding window. In this paper, we choose the feature set which includes: mean absolute value (MAV), waveform length ($WLEN$), zero crossings (ZC) and slope sign changes (SSC). The definition of these features is listed in Table 2. We can know that each vector of features is 8-dimension, which consists of 4 features on each signal channel.

TABLE 2
THE DEFINITION OF FEATURES

$\text{MAV} = \frac{1}{\text{N}}\sum_{i=1}^{\text{N}} \lvert \text{x}_i \rvert$
$\text{ZC} = \sum_{i=1}^{\text{N}} f_i; \quad f_i = \begin{cases} 1 & \text{if } \text{x}_i * \text{x}_{i+1} < 0 \text{ and } \lvert \text{x}_i - \text{x}_{i+1} \rvert \geq \varepsilon \\ 0 & \text{else} \end{cases}$
$\text{SSC} = \sum_{i=1}^{\text{N}} g_i; \quad g_i = \begin{cases} 1 & \text{if } (\text{x}_i - \text{x}_{i-1})(\text{x}_i - \text{x}_{i+1}) > 0, \\ & \lvert \text{x}_i - \text{x}_{i-1} \rvert \geq \varepsilon, \text{and } \lvert \text{x}_i - \text{x}_{i+1} \rvert \geq \varepsilon \\ 0 & \text{else} \end{cases}$
$\text{WL} = \sum_{i=1}^{\text{N}} \lvert \triangle \text{x}_i \rvert; \quad \triangle \text{x}_i = \text{x}_i - \text{x}_{i-1}$

C. Feature classification based on AdaBoostSVM

It is well known that the weak classifiers in AdaBoost is SVM with the RBF kernel, and SVM algorithm is of a very high accuracy in pattern recognition. However the proposed AdaBoostSVM was proven with better generalization performance than SVM on imbalanced classification problems [21].

Traditional RBFSVM compoment classifiers chooses a large σ value (implying weak learning) on the initialization, the σ values would converge as the Boosting iteration proceeds. It would lead to a set of RBFSVM component classifiers with better generalization using a fixed (optimal) σ value, whose model parameters are adaptively different.

However, AdaBoostSVM updates the weights of training samples through the called re-weighting technique. At initialization, a large value is selected for σ, which is similar to a RBFSVM classifier with very weak learning ability. Then, RBFSVM with σ is trained as many steps until more than half accuracy can be achieved. Otherwise, we can regulate this σ value decreased slightly such that the learning capability of RBFSVM is increased to enhance more than half accuracy.

The accuracy of new RBFSVM would not be too strong for the current weighted training samples through decreasing the σ value slightly, and thus we can obtain moderately accurate RBFSVM component classifiers. These larger diversities may lead to a better generalization performance of AdaBoost. This process continues until the σ is decreased to the given minimal value.

Algorithm 1 :The Process of AdaBoostSVM

1.Input: The training samples are labeled as $(x_1, y_1), ..., (x_N, y_N)$; select the initial σ, σ_{ini}, the minimal σ, σ_{min}, the step of σ, and σ_{step}.
2.Initialize: the weights of training samples are chosen as : $w_i^1 = 1/N$, for all $i = 1, \ldots, N$.
3.Do While($\sigma < \sigma_{min}$)
(1) A RBFSVM component classifier is trained, h_t, on the weighted training set.
(2) The training error of h_t is chosen : $\epsilon_t = \sum_{i=1}^{N} w_i^t, y_i \neq h_t(x_i)$;
(3) If $\epsilon_t > 0.5$, choose σ value as σ_{step} and goto (1).
(4) Choose weight for the component classifier h_t: $\alpha_t = \frac{1}{2} ln(\frac{1-\epsilon_t}{\epsilon_t})$
(5) Update the weights of training samples: $w_i^{t+1} = \frac{w_i^t exp(-\alpha_t y_i h_t(x_i))}{C_t}$, i = 1,...,N.
4.Output: f(x) = sign($\sum_{t=1}^{T} \alpha_t h_t(x)$).

V. HYBRID MOTION AND FORCE OPTIMIZATION

A. Kinematics Redundant Resolution Formulation

Consider a bionic arm and denote the the transformation of joint space vector $q \in R^n$ to end-effector's relative position vector $\chi \in R^\varrho$ with $\dot{q} = [\dot{q}_1^T, \ldots, \dot{q}_n^T]^T \in R^n$, where $\dot{q}_i$ is the joint velocity. The kinematic redundancy resolution is to find the set of joint velocity, which are feasible with respect to the kinematic structure of the bionic arm, the corresponding joint position and velocity limits, and minimize the joint velocity. The balance equation for the generalized forces applied to the object can be written in the form

$$J(q)\dot{q} = \dot{\chi} \tag{4}$$

where $J(q) \in R^{n \times \rho}$ is the Jacobian matrix.

In this paper, the constraints of position and velocity can be represented by

$$q_{min} \leqslant q(t) \leqslant q_{max} \tag{5}$$

$$\dot{q}_{min} \leqslant \dot{q}(t) \leqslant \dot{q}_{max} \tag{6}$$

where q_{min} and q_{max} are the boundedness of the joint position, and $\dot{q}_{min}$ and $\dot{q}_{max}$ are the boundedness of the joint velocity.

The inequalities (5) and (6) can also be described by the positive definite matrix

$$K(q, \dot{q}) = \text{diag}(P, V) > 0 \tag{7}$$

where

$$P = \begin{bmatrix} P_{B,L} \\ P_{B,H} \end{bmatrix} = \begin{bmatrix} q - q_{min} \\ -q + q_{max} \end{bmatrix} \tag{8}$$

$$V = \begin{bmatrix} V_{B,L} \\ V_{B,H} \end{bmatrix} = \begin{bmatrix} \dot{q} - \dot{q}_{min} \\ -\dot{q} + \dot{q}_{max} \end{bmatrix} \tag{9}$$

which contains the kinematic constraints from the lower limits $P_{B,L}$, $V_{B,L}$ and upper limits $P_{B,H}$, $V_{B,H}$, respectively.

Hence, we can denote the simultaneous satisfaction of the constraints of both position and joint velocity as

$$K(q, \dot{q}) = \text{diag}(P, V) > 0 \tag{10}$$

The optimization problem is defined based on the minimization of the cost function $\Phi(q, \dot{q})$ as:

$$\Phi(q, \dot{q}) = \dot{q}^T Q \dot{q}/2 + b^T(q(t) - q(0)) \tag{11}$$

$$\text{subject to} \quad J(q)x = \dot{\chi}, \tag{12}$$

$$\xi_{min} \leqslant K(q, \dot{q}) \leqslant \xi_{max}, \tag{13}$$

where Q is symmetric positive definite matrix, and ξ_{min} and ξ_{max} are the boundedness of the position and velocity.

B. Grasping-Force Optimization Formulation

Consider an object grasped by a multi-fingered robotic hand, there exist l contact points between the object and the fingertips, the contact wrench of the grasp is denoted by $f = [f_1^T, \ldots, f_l^T]^T \in R^{lk}$ with the i-th contact vector $f_i \in R^k$ in dimension k, and the generalized external force acting on the object is denoted by $f_e \in R^6$.

In this paper, we assume the point contact model with friction is adopted and the joint actuators could provide the required torques. The contact wrench consists of three vectors: the normal component $f_{i,z}$ to the object surface, and the two components $f_{i,x}$, $f_{i,y}$ on the tangent plane. The friction and joint torque constraint can be described by

$$\frac{1}{\mu_i}\sqrt{f_{i,x}^2 + f_{i,y}^2} \leq f_{i,z} \tag{14}$$

$$\tau_L \leq \tau \leq \tau_U \tag{15}$$

with the tangential friction coefficient μ_i at the i-th contact point, the lower τ_L and upper joint torque bound τ_U, respectively.

Then, we can obtain the following relationship as

$$f_e = Gf \tag{16}$$

$$J^T(q)f + \tau_e = \tau \tag{17}$$

where the grasping matrix $G \in R^{6\times lk}$ is full rank for force-closure grasps, the external torque τ_e includs gravity, Coriolis, centripetal and inertia effects at the fingers joints, τ is the actuator torque, and $J(q) \in R^{lk\times p}$ is the hand Jacobian matrix with the total number of the hand joints p.

Therefore, the grasping force optimization problem can be formulated as finding the optimal grasp wrench minimizing the internal forces acting on the object, under the above constraints. The internal forces are contact wrenches that satisfy the friction cone constraints and belong to the null space of the grasp matrix G.

The frictional inequalities (14) can be described by

$$F(c) = \text{diag}[F_1(f_1), \ldots, F_n(f_n)] > 0 \tag{18}$$

where $F_i(f_i)$ is the symmetric (2×2) matrix

$$F_i(c_i) = \begin{bmatrix} f_{i,z} + \frac{f_{i,x}}{\mu_i} & \frac{f_{i,y}}{\mu_i} \\ \frac{c_{i,y}}{\mu_i} & f_{i,z} - \frac{f_{i,x}}{\mu_i} \end{bmatrix} \tag{19}$$

Similarly, the torque limit constraint (15) can also be described by

$$T(f, q, \tau_e) = \text{diag}(\tau_B) > 0 \tag{20}$$

where

$$\tau_B = \begin{bmatrix} \tau_{B,L} \\ \tau_{B,H} \end{bmatrix} = \begin{bmatrix} J^T(q)f - \tau_L + \tau_e \\ -J^T(q)f + \tau_h - \tau_e \end{bmatrix} \tag{21}$$

with the lower limit $(\tau_{B,L})$ and upper limit $(\tau_{B,H})$, respectively.

Hence, we can denote the simultaneous satisfaction of both frictional and joint torque constraints as the positive definiteness of the linearly constrained block-diagonal matrix

$$\mathcal{T} = \text{diag}(F, T) > 0 \tag{22}$$

Let $f(F)$ be the contact wrench vector extracted from the frictional constraint matrix, and $\tau_B(T)$ as the vector composed by the diagonal elements of T , and $\zeta(\mathcal{T}) = [f(F)^T, \tau_B(T)^T]^T$, the linear constraints on matrix $\mathcal{T}$ can be described as

$$A\zeta(\mathcal{T}) = b \tag{23}$$

with $A = \begin{bmatrix} G & 0 & 0 \\ J^T(q) & -I & 0 \\ J^T(q) & 0 & I \end{bmatrix}$, and $b = \begin{bmatrix} f_e \\ \tau_L - \tau_e \\ \tau_H - \tau_e \end{bmatrix}$, the null matrix is 0 and the identity matrix of proper dimension is I.

Through minimizing the cost function $\Phi(\mathcal{T})$, the optimization can be defined as:

$$\Phi(\mathcal{T}) = \mathcal{T}^T Q \mathcal{T} + b^T \int_0^t \mathcal{T}(t)dt \tag{24}$$

$$\text{subject to} \quad A\zeta(P) = b, \tag{25}$$

$$\xi_{min} \leqslant \mathcal{T} \leqslant \xi_{max}, \tag{26}$$

where Q is symmetric positive definite matrix, and ξ_{min} and ξ_{max} are the boundedness of $\mathcal{T}$.

C. Neuro-dynamics Optimization

Considering the motion optimization (11)–(13) and force optimization (24)–(26), the following constrained hybrid motion-force optimization scheme for bionic arm can be summarized as

$$\begin{aligned} \text{minimize} \quad & X^T Q X + \lambda \int_0^t X(t)dt && (27)\\ \text{subject to} \quad & \mathcal{J}X = \Upsilon && (28)\\ & \xi^- \le X \le \xi^+ && (29) \end{aligned}$$

where $X \in R^n$, $Q \in R^{n\times n}$ is a symmetric positive definite matrix, $\lambda > 0$, $\xi^- \in R^n$ and $\xi^+ \in R^n$ are the lower and upper limits of the a joint variable vector for the motion optimization or grasping for force optimization, respectively, and $\mathcal{J}$ is the corresponding Jacobian matrix.

The dual decision variables can help solve quadratic programming problem (27)-(29) effectively with duality theory. First, according to the Lagrange method [22], [23], defining ω as the m-dimensional ∞ numerically and $y \in R^m$ as the dual decision vector defined for (28).

Quadratic program (27)-(29) merged with a bound constraint can be defined as the linear variational inequalities problem, and we need to get the primal-dual equilibrium variable, then the optimization functions (27)-(29) can be transformed as a set of linear variational inequalities, and to find a primal-dual equilibrium vector $X^* \in n$, $y^* \in m$, e.g.,

$$\begin{bmatrix} X^* \\ y^* \end{bmatrix} \in \Omega = \left\{ \begin{bmatrix} X \\ y \end{bmatrix} | \begin{bmatrix} \xi^- \\ -\omega \end{bmatrix} \le \begin{bmatrix} X \\ y \end{bmatrix} \le \begin{bmatrix} \xi^+ \\ +\omega \end{bmatrix} \right\} \subset R^{n+m} \quad (30)$$

Then, we have

$$\begin{aligned} &\left(\begin{bmatrix} X \\ y \end{bmatrix} - \begin{bmatrix} X^* \\ y^* \end{bmatrix} \right)^T \cdot \left(\begin{bmatrix} I & -J^T \\ J & 0 \end{bmatrix} \cdot \right.\\ &\left. \begin{bmatrix} X^* \\ y^* \end{bmatrix} + \begin{bmatrix} \lambda \int_0^t X(s)ds \\ -\Upsilon \end{bmatrix} \right) \ge 0, \forall \begin{bmatrix} X \\ y \end{bmatrix} \in \Omega \end{aligned} \quad (31)$$

where $I \in R^{n\times n}$. Inspired by the work in [23], it is easy to know that linear variational inequality problem (31) is equivalent to the system of piecewise-linear equations, e.g.,

$$\begin{aligned} P_\Omega \left(\begin{bmatrix} X \\ y \end{bmatrix} - \left(\begin{bmatrix} I & -J^T \\ J & 0 \end{bmatrix} \cdot \begin{bmatrix} X \\ y \end{bmatrix} + \right. \right.\\ \left. \left. \begin{bmatrix} \lambda \int_0^t X(s)ds \\ -\Upsilon \end{bmatrix} \right) \right) - \begin{bmatrix} X \\ y \end{bmatrix} = 0 \end{aligned} \quad (32)$$

where $P_\Omega(.) : R^{n+m} \to \Omega$ is a projection operator. Then, from [30], the linear projection equation (32) can be computed by the following recurrent neural network as

$$\begin{aligned} \begin{bmatrix} \dot{X} \\ \dot{y} \end{bmatrix} &= \gamma \left(E + \begin{bmatrix} I & \mathcal{J} \\ -\mathcal{J}^T & 0 \end{bmatrix} \right) \left\{ P_\Omega \left(\begin{bmatrix} X \\ y \end{bmatrix} - \left(\right. \right. \right.\\ &\left. \left. \left. \begin{bmatrix} I & -\mathcal{J}^T \\ \mathcal{J} & 0 \end{bmatrix} \begin{bmatrix} X \\ y \end{bmatrix} + \begin{bmatrix} \lambda \int_0^t X(s)ds \\ -\Upsilon \end{bmatrix} \right) \right) \right.\\ &\left. - \begin{bmatrix} X \\ y \end{bmatrix} \right\} \end{aligned} \quad (33)$$

where $\gamma > 0$ is designed parameters, which is used to scale the convergence rate, and $E \in R^{(n+m)\times(n+m)}$ is an identity matrix.

Theorem 5.1: Consider any initial states, the state vector $[X^*, y^*]^T$ of the recurrent neural network (33) converges to an equilibrium point $[X^*, y^*]^T$, of which the first n elements constitute the optimal solution X^* to the original QP problem (27)-(29). The exponential stability can be achieved, provided there exists a constant $\sigma > 0$ such that

$$\begin{aligned} &\left\| \begin{bmatrix} X \\ y \end{bmatrix} - P_\Omega \left(\begin{bmatrix} X \\ y \end{bmatrix} - \left(\begin{bmatrix} I & -\mathcal{J}^T \\ \mathcal{J} & 0 \end{bmatrix} \cdot \begin{bmatrix} X \\ y \end{bmatrix} \right. \right. \right.\\ &\left. \left. \left. + \begin{bmatrix} \lambda \int_0^t X(s)ds \\ -\Upsilon \end{bmatrix} \right) \right) \right\|_2^2\\ &\ge \sigma \left\| \begin{bmatrix} X \\ y \end{bmatrix} - \begin{bmatrix} X^* \\ y^* \end{bmatrix} \right\|_2^2 \end{aligned} \quad (34)$$

Proof: A Lyapunov function candidate can be defined as, where the $\|\cdot\|_2^2$ denotes denotes the square of Euclidean two-norm.

$$V \begin{pmatrix} X \\ y \end{pmatrix} = \left\| \begin{bmatrix} X \\ y \end{bmatrix} - \begin{bmatrix} X^* \\ y^* \end{bmatrix} \right\|_2^2 \ge 0$$

Its time derivative along the neural network trajectory (33) can be obtained

$$\begin{aligned} \tfrac{dV}{dt} &= \left(\begin{bmatrix} X \\ y \end{bmatrix} - \begin{bmatrix} X^* \\ y^* \end{bmatrix} \right)^T \gamma \left(E + \begin{bmatrix} I & \mathcal{J} \\ -\mathcal{J}^T & 0 \end{bmatrix} \right.\\ &\left. \right) \times \left\{ P_\Omega \begin{bmatrix} X \\ y \end{bmatrix} - \left(\begin{bmatrix} I & \mathcal{J} \\ -\mathcal{J}^T & 0 \end{bmatrix} \begin{bmatrix} X \\ y \end{bmatrix} \right.\right.\\ &\left.\left. + \begin{bmatrix} \lambda \int_0^t X(s)ds \\ -\Upsilon \end{bmatrix} \right) \right) - \begin{bmatrix} X \\ y \end{bmatrix} \right\}\\ &\le -\gamma \left\| \begin{bmatrix} X \\ y \end{bmatrix} - P_\Omega \left(\begin{bmatrix} X \\ y \end{bmatrix} - \left(\begin{bmatrix} I & \mathcal{J} \\ -\mathcal{J}^T & 0 \end{bmatrix} \begin{bmatrix} X \\ y \end{bmatrix} \right) \right.\right.\\ &\left.\left. + \begin{bmatrix} \lambda \int_0^t X(s)ds \\ -\Upsilon \end{bmatrix} \right) \right) \right\|_2^2\\ &- \gamma \left\| \left(\begin{bmatrix} X \\ y \end{bmatrix} - \begin{bmatrix} X^* \\ y^* \end{bmatrix} \right) \right\|_2^2 \le 0 \end{aligned}$$

From [30], [23], the network state $[X(t), y]^T$ can be stable and globally convergent to an equilibrium $[X^*, y^*]^T$ in view of $\dot{V} = 0$ when $[X^*, y^*]^T = 0$ and $[X, y]^T = [X^*, y^*]^T$. It can be obtained that the first n elements of $[X^*, y^*]^T$ are the

optimal solution to the optimization function (27)-(29). As for the exponential convergence, review $V([X,y]^T), \dot{V}([X,y]^T)$, and the extra condition

$$\frac{dV\left(\begin{bmatrix} X \\ y \end{bmatrix}\right)}{dt} \leq -\gamma\left(\begin{bmatrix} X \\ y \end{bmatrix} - \begin{bmatrix} X^* \\ y^* \end{bmatrix}\right)^T \cdot \left(\sigma E + \begin{bmatrix} I & \mathcal{J} \\ -\mathcal{J}^T & 0 \end{bmatrix}\right) \cdot \left(\begin{bmatrix} X \\ y \end{bmatrix} - \begin{bmatrix} X^* \\ y^* \end{bmatrix}\right) \leq -\lambda V\left(\begin{bmatrix} X \\ y \end{bmatrix}\right)$$

where $\lambda = \sigma\gamma > 0$ is convergence rate. Thus, $V([X]^T) = O(exp(-\lambda(t-t_0)))$; $\forall t \geq t_0$ can be obtained, and hence

$$\left\| \begin{bmatrix} \int_0^t X(t)dt \\ y \end{bmatrix} - \begin{bmatrix} \int_0^t X^* dt \\ y^* \end{bmatrix} \right\|_2^2 = O(\exp(-\lambda(t-t_0)/2))$$

where $\forall t \geq t_0$, which completes the proof of exponential stability. ■

VI. Experiment Verification

To verify the effectiveness of the proposed approaches, our developed 5-degrees-of-freedom (DOF) bionic arm is utilized in the experiments. In the actual implementation, the sampling period is chosen as 50 ms. In the experiment, we choose three hand postures-relaxing, full extension and grasping. First, the selected subject participates in the sEMG signal collection, there are the four sEMG sensors attached to the subject's forearm, as shown in Fig. 8. Fig. 9 shows the three specific gesture: relaxing, grasping and full extension. During training, each posture is held for 7s with 5s rest. The collected sEMG signals are shown in Figs. 10–12, respectively. After training, SVM classifier would label three postures as following: 0 for relaxing, 1 for grasping, 2 for full extension. Actually, only three fingers, for example, thumb, index finger, middle finger, are involved in the experiment. There are four kinds of features extracted from 4 channels of sEMG signals, shown in Tab. 2. The four features were extracted from the segmented samples, and then used for training the feature projected matrices. Fig. 19 shows the accuracy and error rates of the three label classification.

The Bumblebee 2 is placed on the top of the bionic shown in Fig. 1 such that the marker on the object can be tracked within the range of the camera perspective. Both cameras work at 20 frames per second and are calibrated before the experiments. The target object and the thumb of the hand have one circular features (red dots), respectively, shown in Fig. 7. The trajectory and position of the objects are chosen carefully to ensure the visibility of the objects for the cameras. Fig. 20 shows the region labeled by the black lines of the 3D point cloud. The one of the red marker is the target object position, and the other is the initial position of the end-effector.

By detecting the five colored circular blobs of the particular mark, image coordinates of the feature point can be robustly obtained by considering the color information and the known geometrical relationship among different blobs. Furthermore, through the use of image coordinates of the geometrical centers of the colored circular blobs, the orientation angle of

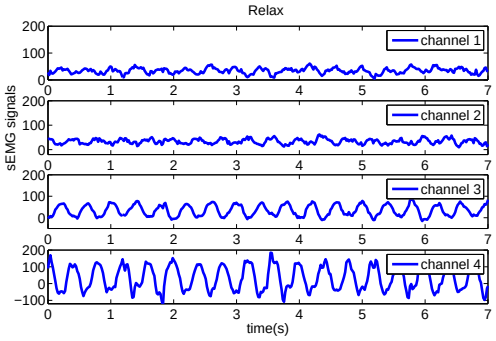

Fig. 10. sEMG signals in the relax status.

the bionic arm on the image plane can also be calculated in each control cycle. By considering the approximated distance of the camera as the depth of the feature point, we can easily reconstruct the Cartesian coordinates of the feature point in the camera frame using its image coordinates and the calibrated values of camera intrinsic parameters. In the experiments, the initial image coordinates and corresponding reconstructed Cartesian coordinates of the feature point are required to be stored for calculating the position and orientation of the end-effector.

The proposed motion optimization scheme (11)–(13) with $\lambda = 3$ is used, where $\Gamma = 10^{10}$. The task duration time is 6 s, and the initial joint variables $q(0) = [0.1\pi, 0.1\pi, 0.1\pi, 0]$ in radians. The center of the bionic palm is the position of the end-effector. The length of three links are: $[26.50, 33.50, 15.00]^T$cm, $n = 4$, $m = 3$. Figs .13–15 show the curves of three joints tracking in joint space, respectively. The position tracking trajectories in task space are presented in Figs. 16–18, respectively. From Figs. 13–18, it is shown that the real trajectories converges to the desired trajectories. Fig. 21 shows the real trajectory. The grasping model is defined by the position of three grasp points: $p_T = [2.00, -11.00, 2.00]^T$mm; $p_I = [-11.00, 11.00, 2.00]$mm; $p_M = [15.00, 11.00, 2.00]$ mm. The scaling parameter $\lambda_f = 1000$. The transformation matrix G can be described as

$$G^T = \begin{bmatrix} 0 & 0 & 1 & -0.011 & -0.002 & 0 \\ 1 & 0 & 0 & 0 & 0.002 & 0.011 \\ 0 & 1 & 0 & -0.002 & 0 & 0.002 \\ 1 & 0 & 0 & 0 & 0.002 & -0.011 \\ 0 & 0 & 1 & 0.011 & 0.011 & 0 \\ 0 & -1 & 0 & 0.002 & 0 & 0.011 \\ 1 & 0 & 0 & 0 & 0.002 & -0.011 \\ 0 & 0 & 1 & 0.011 & -0.015 & 0 \\ 0 & -1 & 0 & 0.002 & 0 & -0.015 \end{bmatrix}$$

Force optimization solution can be solved with (24). The mass of the target object is $m = 0.51kg$. The friction coefficient is chosen as $\mu_i = 0.8$. We can calculate the corresponding torque of each finger. By using the feedback of the force sensor, we regulate the contact forces. Figs. 24-25 show the optimized contact force and control input motor currents.

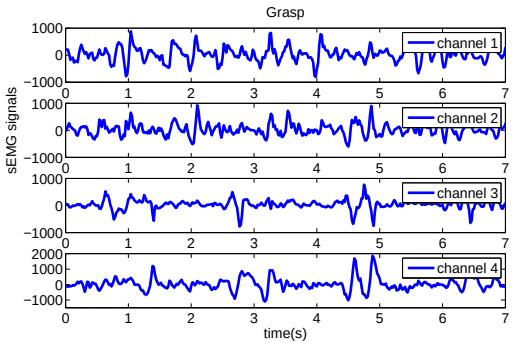

Fig. 11. sEMG signals in the grasp status.

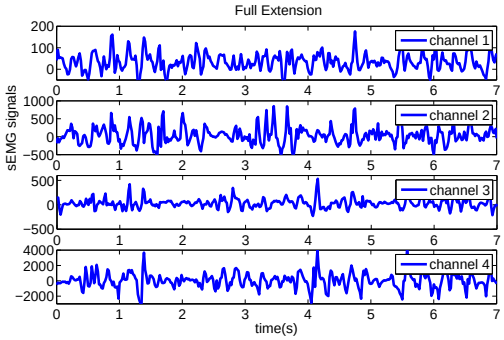

Fig. 12. sEMG signals in the extension status.

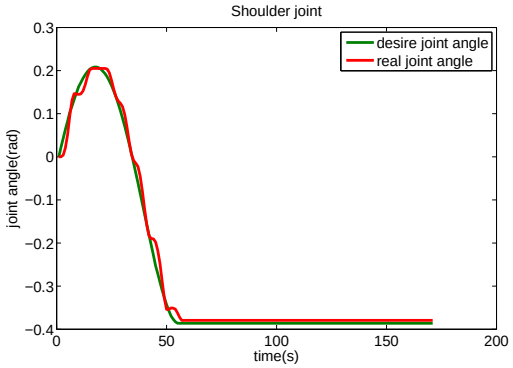

Fig. 13. Shoulder joint angle

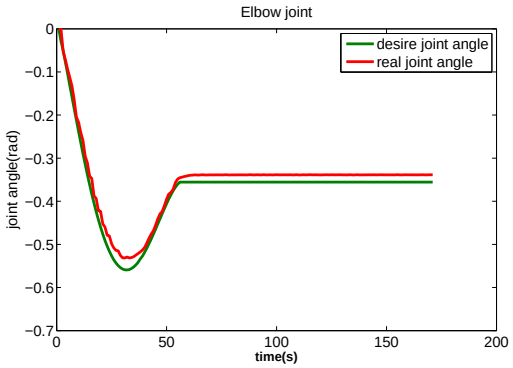

Fig. 14. Elbow joint angle

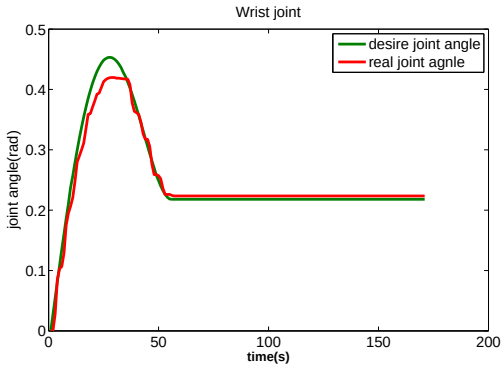

Fig. 15. Wrist joint angle

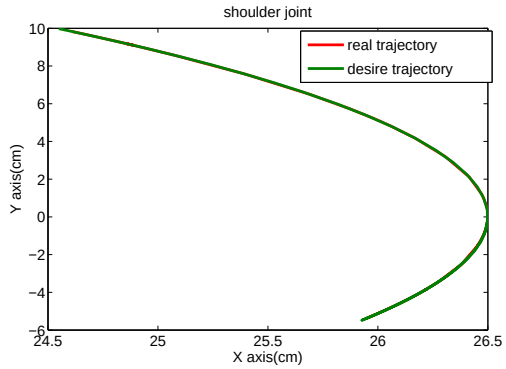

Fig. 16. Shoulder joint trajectory

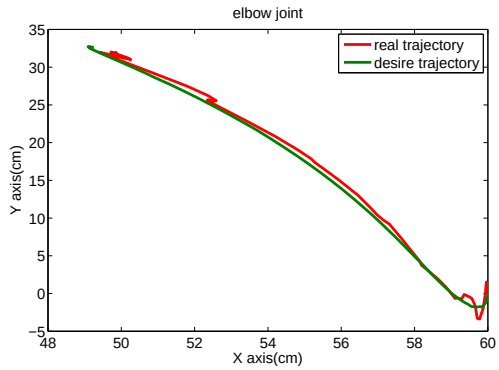

Fig. 17. Elbow joint trajectory

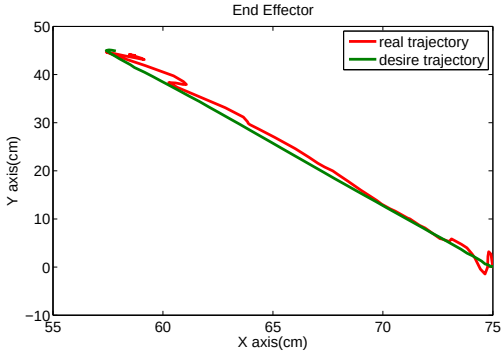

Fig. 18. End-Effector trajectory

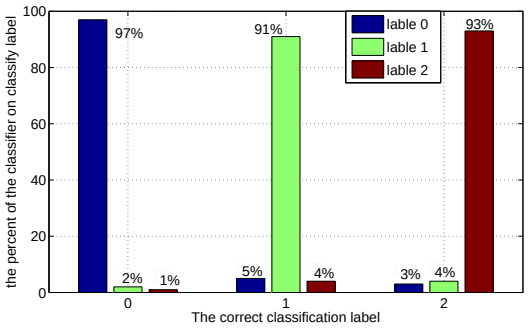

Fig. 19. The result of the classification

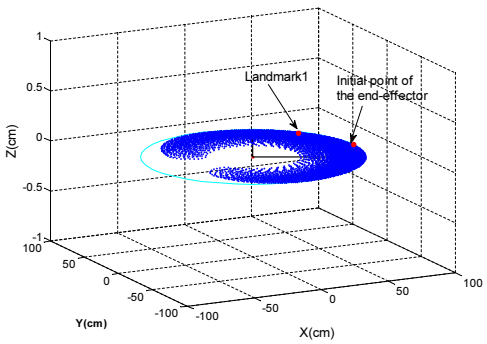

Fig. 20. Cloud of reachable points

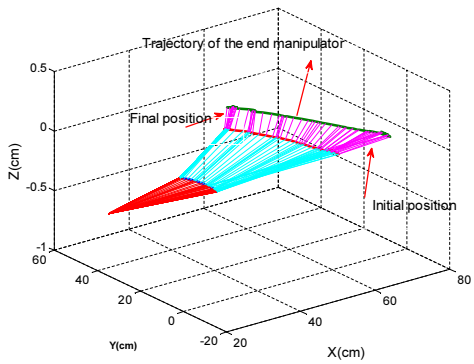

Fig. 21. Manipulator Trajectory

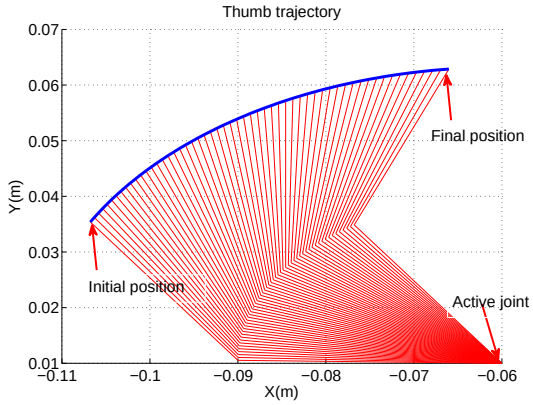

Fig. 22. Thumb trajectory

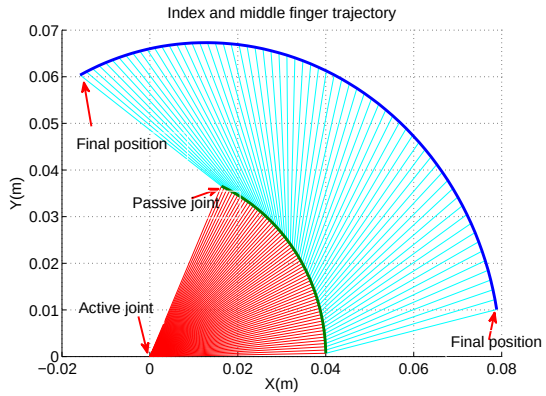

Fig. 23. Index and Middle fingers trajectory

VII. Conclusion

In this paper, a sensory-motor fusion based manipulation and grasping control for a robotic hand-eye system is developed, and it consists of three modules: vision servoing, sEMG-based movement cognition, and hybrid force and motion optimization for manipulation and grasping. The stereo camera is used to obtain the 3D point cloud of a target object and provides the desired operational position. The AdaBoost-SVM

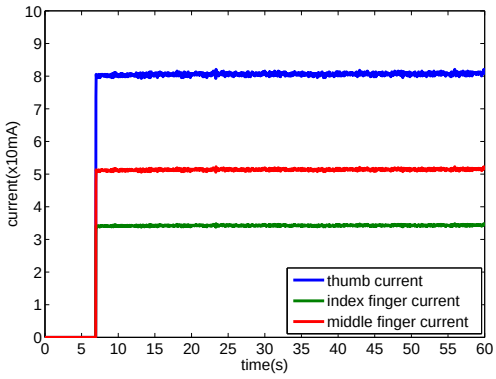

Fig. 24. Three fingers current

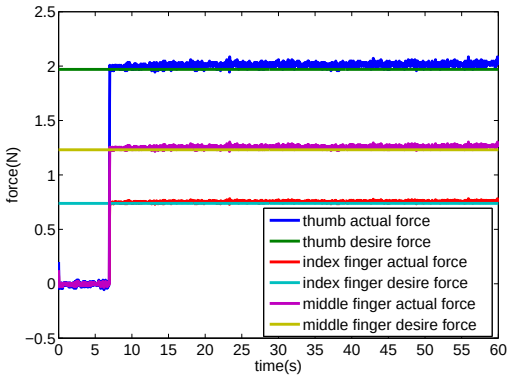

Fig. 25. Three fingers force

based motion recognition is proposed to discriminate different movements based on sEMG of the multi-fingered robotic hand. The operational space motion planning for bionic arm and force planning for multi-fingered robotic hand can be both transformed as a convex optimization problem, considering also various constraints. A neural dynamics optimization solution is proposed and is suitable to be implemented online. Real-time experiments are conducted and the results exhibit the responsiveness and flexibility of the proposed approach.

REFERENCES

[1] R. de Souza, S. El-Khoury, J. Santos-Victor, A. Billarda, "Recognizing the grasp intention from human demonstration," *Robotics and Autonomous Systems*, vol. 74, Part A, 2015, pp. 108-121.

[2] C. Cipriani , M. Controzzi , M. C. Carrozza "The SmartHand transradial prosthesis," *Journal of NeuroEngineering and Rehabilitation*, vol. 8, no. 29, 2011, pp. 1-13.

[3] X. Chen, D. Zhang, and X. Zhu, "Application of a self-enhancing classification method to electromyography pattern recognition for multifunctional prosthesis control," *Journal of NeuroEngineering and Rehabilitation*, vol. 10, no. 1, 2013, pp. 1-44.

[4] A. D. Roche, H. Rehbaum, D. Farina, and O. C. Aszmann, "Prosthetic myoelectric control strategies: A clinical perspective," *Current Surgery Reports*, vol. 2, no. 3, Mar 2014, pp. 1-11.

[5] C. Cipriani, F. Zaccone, S. Micera, and M. Carrozza, "On the shared control of an EMG-controlled prosthetic hand: analysis of user prosthesis interaction," *IEEE Transactions on Robotics*, vol. 24, no. 1, Feb 2008, pp. 170-184.

[6] A. J. Young, L. H. Smith, E. J. Rouse, and L. J. Hargrove, "A comparison of the real-time controllability of pattern recognition to conventional myoelectric control for discrete and simultaneous movements," *Journal of NeuroEngineering and Rehabilitation*, vol. 11, no. 1, 2014, pp. 1-5.

[7] M. Ortiz-Catalan, B. Hakansson, and R. Branemark, "Real-time and simultaneous control of artificial limbs based on pattern recognition algorithms," *IEEE Transactions on Neural Systems and Rehabilitation Engineering*, vol. 22, no. 4, July 2014, pp. 756-764.

[8] J. Hahne, F. BieBmann, N. Jiang, H. Rehbaum, D. Farina, F. Meinecke, K.-R. Muller, and L. Parra, "Linear and nonlinear regression techniques for simultaneous and proportional myoelectric control," *IEEE Transactions on Neural Systems and Rehabilitation Engineering*, vol. 22, no. 2, 2014, pp. 269-279.

[9] E. Scheme, A. Fougner, A. Chan, and K. Englehart, , "Examining the adverse effects of limb position on pattern recognition based myoelectric control," in *Engineering in Medicine and Biology Society (EMBC), Annual International Conference of the IEEE*, 2010, pp. 6337-6340.

[10] P. K. Artemiadis and K. J. Kyriakopoulos, "An EMG-Based Robot Control Scheme Robust to Time-Varying EMG Signal Features," *IEEE Transactions on Information Technology in Biomedicine*, vol. 14, no. 3, May 2010, pp. 582-588.

[11] L. Hargrove, K. Englehart, and B. Hudgins, "The effect of electrode displacements on pattern recognition based myoelectric control," *28th Annual International Conference of the IEEE in Engineering in Medicine and Biology Society*, 2006, pp. 2203-2206.

[12] A. Gijsberts, R. Bohra, D. Sierra Gonzalez, A. Werner, M. Nowak, B. Caputo, M. A. Roa, and C. Castellini, "Stable myoelectric control of a hand prosthesis using non-linear incremental learning," *Frontiers in Neurorobotics*, vol. 8, no. 8, pp. 1-15, 2014.

[13] J. W. Sensinger, B. A. Lock, and T. A. Kuiken, "Adaptive pattern recognition of myoelectric signals: exploration of conceptual framework and practical algorithms," *IEEE Transactions on Neural Systems and Rehabilitation Engineering*, vol. 17, no. 3, 2009, pp. 270-278.

[14] P. M. Pilarski, M. R. Dawson, T. Degris, F. Fahimi, J. P. Carey, and R. S. Sutton, "Online human training of a myoelectric prosthesis controller via actor-critic reinforcement learning," *2011 IEEE International Conference on Rehabilitation Robotics*, 2011, pp. 1-7.

[15] R. Khushaba, "Correlation analysis of electromyogram signals for multiuser myoelectric interfaces," *IEEE Transactions on Neural Systems and Rehabilitation Engineering*, vol. 22, no. 4, 2014, pp. 745-755.

[16] V. Kamat, S. Ganesan, "A robust hough transform technique for description of multiple line segments in an image," *Proceedings of the 1998 International Conference on Image Processing*, vol. 1, 1998, pp. 216-220.

[17] J. Kofman, X. Wu, T. Luu, S. Verma, "Teleoperation of a robot manipulator using a vision-based human-robot interface," *IEEE Transactions on Industrial Electronics*, vol. 52, no. 5, 2005, 1206-1219.

[18] C. Yang , S. Amarjyoti, X. Wang, Z. Li, H. Ma, C.-Y. Su, " Visual servoing control of baxter robot arms with obstacle avoidance using kinematic redundancy," *Intelligent Robotics and Applications*, vol. 9244 of the series Lecture Notes in Computer Science, 2015, pp 568-580.

[19] H. Xiao, Z. Li, C. Yang, W. Yuan, L. Wang, " RGB-D sensor based visual-target detection and tracking for an intelligent wheelchair robot in indoors environments," *International Journal of Control, Automation and Systems*, vol. 13, no. 3, June 2015, pp.521-529.

[20] Z. Li, B. Wang, F. Sun, C. Yang, Q. Xie, W. Zhang, "sEMG-based joint force control for an upper-limb power-assist exoskeleton robot," *IEEE Journal of Biomedical and Health Informatics*, vol.18, no. 3, May 2014, pp. 1043-1050.

[21] Z. Li, B. Wang, C. Yang, Q. Xie, C.-Y. Su, "Boosting-based EMG patterns classification scheme for robustness enhancement," *IEEE Journal of Biomedical and Health Informatics*, vol. 17, no. 3, May 2013, pp. 545-552.

[22] Y. Xia, J. Wang, and L.-M. Fok, "Grasping-force optimization for multifingered robotic hands using a recurrent neural network," *IEEE Trans. Robotics and Automation*, vol. 20, no. 3, 2004, pp. 549-554.

[23] Z. Li, S. Xiao, S. S. Ge and H. Su, "Constrained multi-legged robot system modeling and fuzzy control with uncertain kinematics and dynamics incorporating foot force optimization," *IEEE Transactions on Systems Man and Cybernetics: Systems*, vol. 46, no. 1, 2016, pp. 1–15.

[24] S. A. Dalley , T. E. Wiste , T. J. Withrow , M. Goldfarb, "Design of a multifunctional anthropomorphic prosthetic hand with extrinsic actuation," *IEEE/ASME Trans. Mechatronics*, vol. 14, no. 6, 2009, pp. 699-706.

[25] R. Weir , M. Mitchell ,S. Clark, G. Puchhammer , K. Kelley, M. Haslinger ,N. Kumar, R. Hofbauer , P. Kuschnigg , V. Cornelius , M. Eder , R. Grausenburger , "New multifunctional prosthetic arm and hand systems," *Proc IEEE EMBS Intl Conf*, 2007, pp. 4359-4360.

[26] B. Hudgins , P. Parker , R. Scott , " Control of artificial limbs using myoelectric pattern recognition," *Med Life Sci Eng*, vol. 13, 1994, pp. 21-38.

[27] H. Su, B. He, "A simple rectification method of stereo image pairs with calibrated cameras," In: *2010 2nd International Conference on Information Engineering and Computer Science* (ICIECS), 2010, pp. 1-4.

[28] H. Hirschmuller, "Accurate and efficient stereo processing by semi-global matching and mutual information." *IEEE Computer Society Conference on Computer Vision and Pattern Recognition*, vol. 2, no. 7, Jun. 2005, pp. 807-814.

[29] M. S. Bazaraa, H. D. Sherali, and C. M. Shetty, *Nonlinear programming: theory and algorithms*, New York, NY, USA: Wiley, 2013.

[30] Z. Zhang and Y. Zhang, "Acceleration-level cyclic-motion generation of constrained redundant robots tracking different paths," *IEEE Trans. Syst., Man, Cybern. Part B: Cybern.*, vol. 42, no. 4, Aug. 2012, pp. 1257-1269.

[31] Z. Li, C. Yang, C.-Y. Su, J. Deng, W. Zhang, "Vision-based model predictive control for steering of a nonholonomic mobile robot," *IEEE*

Transactions on Control Systems Technology, vol. 24, no. 2, 2016, pp. 553-564.
[32] W. He, Y. Dong, C. Sun, "Adaptive neural impedance control of a robotic manipulator with input saturation," *IEEE Transactions on Systems Man and Cybernetics: Systems*, vol. 46, no. 2, 2016, pp. 334–344.
[33] Z. Li, H. Xiao, C. Yang, Y. Zhao, "Model predictive control of nonholonomic chained systems using general projection neural networks optimization," vol. 45, no. 10, 2015, pp. 1313–1321.
[34] E. A. Al-Gallaf, "Neuro-kinematics based dexterous robotics hand force optimization, " *Journal of Intelligent and Robotic Systems*, vol. 50, no. 2, pp. 181-206, Oct. 2007.

Yingbai Hu received the B.S. degree in automation from Hubei University of Technology, Hubei, China, in 2014. He is currently pursuing the master's degree with the College of Automation Science and Engineering, South China University of Technology, Guangzhou, China. He has authored one paper in international conferences. His current research interests include bionic arms and prosthesis hands, and electromyography (EMG) signals processing.

Zhijun Li (M'07-SM'09) received the Ph.D. degree in mechatronics, Shanghai Jiao Tong University, P. R. China, in 2002. From 2003 to 2005, he was a postdoctoral fellow in Department of Mechanical Engineering and Intelligent systems, The University of Electro-Communications, Tokyo, Japan. From 2005 to 2006, he was a research fellow in the Department of Electrical and Computer Engineering, National University of Singapore, and Nanyang Technological University, Singapore. From 2007-2011, he was an Associate Professor in the Department of Automation, Shanghai Jiao Tong University, P. R. China. In 2008, he was a visiting scholar in Microsoft Research Asia, Beijing. Since 2012, he is a Professor in College of Automation Science and Engineering, South China university of Technology, Guangzhou, China. In 2015, he is a visiting professor in Faculty Science and Technology, the University of Macau, Macau, China, and Department of Advanced Robotics, Italian Institute of Technology, Genoa, Italy. He is serving as an Editor-at-large of Journal of Intelligent & Robotic Systems, Associate Editors of IEEE Transactions on Neural Networks and Learning Systems and IEEE Transactions on Systems, Man and Cybernetics: Systems. Dr. Li's current research interests include service robotics, tele-operation systems, nonlinear control, neural network optimization, etc.

Guanglin Li (M'01-SM'06) received the B.S. and the M.S. degrees both in electrical engineering from Shandong University, Jinan, China, in 1983 and 1988, respectively, and the Ph.D. degree in biomedical engineering from Zhejiang University, Hangzhou, China, in 1997. From 2006 to 2009, he was a Senior Research Scientist in the Neural Engineering Center for Artificial Limbs at the Rehabilitation Institute of Chicago and, also, a Research Assistant Professor in the Department of Physical Medicine and Rehabilitation at Northwestern University, Chicago. Since 2009, he has been with Shenzhen Institutes of Advanced Technology (SIAT), Chinese Academy of Sciences, Shenzhen, China, where he is currently a Professor in the Research Centre for Neural Engineering at the Institute of Biomedical and Health Engineering. His current research interests include neural rehabilitation engineering, neuroprosthesis control, biomedical signal analysis, and computational biomedical engineering. He is an Associate Editor of the IEEE Journal of Biomedical and Health Informatics and serves as an International Advisory Board member of journal of Physiological Measurement.

Peijiang Yuan received the B.S. degree in department of automation from the Tsinghua University, Beijing, China, in 1997, and Ph.D. degrees in electronic and computer engineering from University of Western Ontario, Canada, in 2005. He joined Beihang University, in 2009. He is currently an associate Professor with the Intelligent Technology and Robotics Research Center in Beihang University. His current research interests include aviation manufacturing robot, robot localization and perception, intelligent control and machine vision. He has authored over 50 papers in international journals and conferences. Dr. Yuan has served for several international conferences as a Program Committee Member, the Program Committee Co-Chair of the 2010 IEEE World Congress on Computational Intelligence and the committee member of 2011 IEEE Robotics and Automation and Intelligent Robots and Systems.

Chenguang Yang (M'10) received the B.Eng. degree in measurement and control from Northwestern Polytechnical University, Xi'an, China, in 2005, and the Ph.D. degree in control engineering from the National University of Singapore, Singapore, in 2010. He is a Senior Lecturer with Zienkiewicz Centre for Computational Engineering, Swansea University, UK. He received postdoctoral training in the Department of Bioengineering at Imperial College London, UK. His major research interests lie in robotics, automation and computational intelligence.

Rong Song received the B.S. degree in electrical engineering from Tsinghua University, Beijing, China, in 1999, the M.S. degree in electronic engineering from Shantou University, Shantou, China, in 2002, and the Ph.D. degree in biomedical engineering from the Hong Kong Polytechnic University, Kowloon, Hong Kong, in 2006. He is currently associate professor in school of engineering, Sun Yat-sen University, P.R. China. His research interests include musculoskeletal modeling, biomedical signal processing, human motion analysis, and robot-assisted stroke rehabilitation.